Journal of Catalysis 258 (2008) 71–82

Contents lists available at ScienceDirect

Journal of Catalysis

www.elsevier.com/locate/jcat

Dehydration of glycerol in gas phase using heteropolyacid catalysts as active compounds

Hanan Atia [a], Udo Armbruster [b], Andreas Martin [b,*]

[a] Faculty of Women for Science, Arts and Education, Ain Shams University, Cairo, Egypt
[b] Leibniz Institut für Katalyse e.V. (branch Berlin), Richard-Willstätter-Str. 12, D-12489 Berlin, Germany

ARTICLE INFO

Article history:
Received 19 March 2008
Revised 24 May 2008
Accepted 29 May 2008
Available online 30 June 2008

Keywords:
Glycerol
Dehydration
Acrolein
Heteropolyacids
Catalysis
Gas phase

ABSTRACT

Different silica-, alumina-, and aluminosilicate-supported heteropolyacid catalysts were prepared using phosphomolybdic acid $H_3PMo_{12}O_{40}\cdot xH_2O$, phosphotungstic acid $H_3PW_{12}O_{40}\cdot xH_2O$, silicotungstic acid $H_4SiW_{12}O_{40}\cdot xH_2O$, and ammonium phosphomolybdate $(NH_4)_3PMo_{12}O_{40}\cdot xH_2O$ as precursor compounds. The as-synthesised solids were characterised by nitrogen adsorption, XRD, TG/DTA, Raman spectroscopy, and TPD of ammonia. Silica-supported heteropolyacids are rather well crystallised, whereas alumina-supported samples are X-ray amorphous. Investigations using Raman spectroscopy of calcined samples and TG/DTA revealed that molybdenum-containing heteropolyacids tend to decompose partly close to 400 °C into molybdates and MoO_3 whereas tungsten-containing samples are stable. This makes in particular tungsten-based materials interesting acid catalysts for the dehydration of glycerol in the gas phase. In particular, the influence of selected support materials, catalyst loading, and temperature on acrolein formation was studied at standardised reaction conditions (10% by weight of glycerol in water, 225–300 °C, modified contact time 0.15 kg h mol^{-1}). Surprisingly, alumina is found to be superior to silica as support material with regard to catalyst activity and selectivity. Nevertheless, tungsten based heteropolyacids showed outstanding performance and stability. Acrolein was always the predominant product with maximum selectivity of 75% at complete conversion over silicotungstic acid supported over alumina and aluminosilicate.

1. Introduction

The rapidly rising production of biodiesel from vegetable oils has led to a drastic surplus of by-product glycerol in the chemical markets. Glycerol production in the US already averages more than 350,000 tons per year and in Europe, its production has tripled within the last ten years to approximately 600,000 tons per year. This may increase further as European Commission implemented EU directive 2003/30/EC which targets at the addition of 5.75% of biofuel to car fuels by the year 2010 [1]. Unfortunately, the current application of glycerol is mainly confined to pharmaceuticals and cosmetics and hence the demand is somewhat limited. The availability of large amounts of cheap glycerol is the driving force to develop new processes for its energetic or chemical utilisation (e.g., [2]). Finding value-added alternatives to glycerol incineration would improve economic viability of biodiesel manufacture and the biofuel supply chain [1].

Chemical utilisation of glycerol might include such attractive chemicals as acrolein, propanediols or epichlorohydrin. Recently, Solvay installed an epichlorohydrin process (Epicerol) using glycerol [3]. An intrinsic problem in glycerol conversion is the presence of primary and secondary hydroxyl groups with different reactivity that induce selectivity problems in redox as well as acid–base reactions. Commercial glycerol oxidation processes using hydrogen peroxide are known to produce glycerol aldehyde [4,5] and dihydroxyacetone as an intermediate for glyceric acid and syrine [6,7] in liquid phase. To overcome the reactivity/selectivity problem, researchers tried to synthesise glycerol derivatives, e.g. acetals or esters that allow the subsequent oxidation of only one type of carbon atom [8]. Hydrogenolysis of glycerol on Ru/C catalysts in the presence of an acidic catalyst like amberlyst leads to 1,2- and 1,3-propanediol at mild reaction conditions [9]. The overall reaction is indeed a combination of dehydration and subsequent hydrogenation via the formation of hydroxyacetone.

The best-known acid catalysed reactions with glycerol are (i) condensation to form linear or cyclic glycerol dimers and oligomers [10,11] and (ii) dehydration to form acrolein and other compounds. To perform the dehydration of glycerol to acrolein, strong catalyst acidity seems to be necessary. Various solid acid catalysts including sulphates, phosphates and zeolites have been tested for the dehydration of glycerol in either gaseous or liquid phases [12–14]. Dehydration of glycerol (and other alcohols) was also carried out in supercritical water ($T > 374$ °C, $p > 221$ bar)

* Corresponding author. Fax: +49 30 6392 4454.
E-mail address: andreas.martin@catalysis.de (A. Martin).

0021-9517/$ – see front matter
doi:10.1016/j.jcat.2008.05.027

with H_2SO_4 (acrolein selectivity of 84% at 40% conversion [15]) or with $ZnSO_4$ as catalyst (75% selectivity at 50% conversion [16]). Acrolein selectivity up to 80% at 90% conversion was reported with H_2SO_4 as catalyst at 400 °C [17]. Studies by Degussa in the mid-nineties showed that the reaction can also be carried out in liquid water at 180–340 °C and in gas phase at 250–340 °C with several acidic catalysts like HZSM-5 or HY zeolites, supported mineral acids, and heteropolyacids. Acrolein yields up to 75% at complete conversion were obtained [13]. Chai et al. communicated the use of sulphated zirconia [18] or Nb_2O_5 [19] but these catalysts did not show better performance. Very recently, Tsukuda et al. [20] tested heteropolyacids supported over SiO_2 and found that the introduction of mesopores in silica support significantly affected the catalytic activity. However, such strongly acidic catalysts deactivate quickly as carbonaceous deposits block the catalyst surface, in particular in the presence of large amounts of micropores.

Heteropolyacids (HPA) are a class of materials with well-defined structures and widely tuneable acidity, making them excellent catalysts for acid–base reactions. Their chemical composition is typically described as $[X^{n+}Y_{12}O_{40}]^{8-n}\cdot xH_2O$ (with X = P, Si, B; Y = Mo, W, V; n = oxidation state of X). Different polyanion structures and molecular arrangements for heteropolyacids exist, like Anderson, Dawson and Keggin structures, but most of the catalytic researchers have focused on the latter type. These solids are soluble in polar solvents and have strong Brønsted acidity as proofed in many studies [21]. Besides that, choice of an appropriate metal Y that owns different oxidation states makes them also active in redox catalysis. Heteropolyacids offer structural flexibility allowing for exchange of water and polar organic molecules. On the other hand, they lack thermal stability and have low specific surface area (1–5 m^2/g). This is the reason why heteropolyacids are often supported over acidic or neutral carriers like Al_2O_3 or SiO_2 [21].

In the present investigation, several supported heteropolyacids (HPA) were prepared, characterised and tested in dehydration of glycerol in gas phase for their catalytic performance. Emphasis was also laid on reaction engineering aspects like selectivity/conversion dependency of the reaction on these catalysts and long-term stability experiments.

2. Experimental

2.1. Catalyst synthesis

Four commercially available heteropolyacids such as phosphomolybdic acid $H_3PMo_{12}O_{40}\cdot xH_2O$ (HPMo, *Merck*), phosphotungstic acid $H_3PW_{12}O_{40}\cdot xH_2O$ (HPW, *Aldrich*), silicotungstic acid $H_4SiW_{12}O_{40}\cdot xH_2O$ (HSiW, *Fluka*) and ammonium phosphomolybdate $(NH_4)_3PMo_{12}O_{40}\cdot xH_2O$ (NH_4PMo, *ABCR*) are used as precursors for preparing supported catalysts by incipient wetness method. More details on the catalyst preparation are described below. Aqueous solutions with calculated amounts of the precursors (10 or 20 wt%) were added separately to solid supports such as Al_2O_3 (pore diameter of 5 nm, support denoted as A5; *Fluka*) and SiO_2 (2 nm, S2; *Fluka*) under stirring for 20 h. Excess water was removed with a rotary evaporator at 60 °C. The samples were dried for 2 h at 120 °C in air and finally calcined at 400 °C for 4 h under airflow. After calcination a prompt usage for catalytic tests was realised. Additionally, the samples were heated before catalytic tests under nitrogen to the desired reaction temperatures to remove physisorbed water.

Another series of catalysts with 20% by weight of silicotungstic acid (HSiW) was supported over aluminosilicate (pore diameter of 4 nm, support denoted as AS4 (Siral® 10); *Condea*), alumina (12 nm, A12; *Fluka*), and silica (11 nm, S11; *Fluka*) (Table 1). All these samples were dried and calcined as described above. The catalysts will be marked as following: the denotation of HPA20/A5 contains the abbreviation of the HPA, 20 or 10 indicates the loading percentage, while A5 represents the type of support and its average pore diameter in nm.

Table 1
Results from BET measurements for catalysts and supports

Material	A_{BET} ($m^2\,g^{-1}$)	Percentage of deviation relative to support	Pore volume ($cm^3\,g^{-1}$)	Average pore diameter (nm)
A5	297.7	–	0.427	4.6
HPMo20/A5	253.5	−14.9	0.293	3.9
HSiW20/A5	249.7	−16.1	0.278	3.8
HPMo10/A5	306.9	+3.1	0.355	4.1
HSiW10/A5	307.0	+3.1	0.361	4.1
A12	292.1	–	1.192	11.9
HSiW20/A12	250.2	−14.3	0.828	11.3
S2	648.8	–	0.327	1.5
HPMo20/S2	418.4	−35.6	0.221	1.6
HSiW20/S2	422.8	−34.8	0.224	1.6
HPMo10/S2	442.0	−31.9	0.237	1.7
HSiW10/S2	528.1	−18.6	0.271	1.7
S11	320.7	–	1.189	11.0
HSiW20/S11	259.5	−19.1	0.925	10.8
AS4	383.6	–	0.527	4.4
HSiW20/AS4	309.2	−19.4	0.398	3.5

2.2. Catalyst characterisation

BET surface area, pore volume, and average pore diameter for fresh and spent solids were derived from nitrogen adsorption isotherms measured at −196 °C (*Micromeritics ASAP 2020*). Before the measurement, each sample was degassed at 200 °C for 4 h. The average pore diameters were calculated according to BJH method.

The X-ray powder diffraction measurements were carried out on a STADI P automated transmission diffractometer (*STOE*, Darmstadt) with $CuK\alpha^1$ radiation and Ge monochromator. The pattern was scanned in the 2θ range of 5–60° (step width 0.5°, 100 s per step) and recorded with a STOE position sensitive detector (PSD). The samples were prepared to flat plates. The phase analysis was carried out with the *Win Xpow* software package, including the powder diffraction file (PDF).

Raman spectroscopic investigations were carried out using a fibre optical RXN-Spectrometer (*Kaiser Optical Systems*, 785 nm Laser) with a Laser power of 50 mW.

Thermogravimetric analysis (TG) of fresh (dried at 120 °C only) as well as of spent catalysts was performed using a *SETARAM TG-DTA 92-12* instrument that allowed both TGA and DTA curves to be recorded simultaneously. The experiments were carried out from room temperature up to 800 °C with a heating rate of 10 K/min under airflow (1 l/h).

TPD of ammonia (TPDA) profiles were measured on a commercial characterisation equipment (*AMI-1, Altamira/Zeton)* under He flow (30 ml/min) with a heating rate of 5 K/min up to 600 °C and 1.5 h hold time. After absorption in 0.05 N H_2SO_4, the total amount of ammonia was quantified by back-titration with 0.05 N NaOH versus Tashiro indicator. The desorption curves were monitored with a thermal conductivity detector (TCD). Desorbed water and possibly desorbed CO_2 were captured in a trap with KOH split before entering the TCD. Prior to recording the curves the samples were heated to 400 °C (10 K/min) and held for 1 h under flowing He.

2.3. Catalytic tests

The glycerol dehydration tests were realised in a continuous flow apparatus as shown in Fig. 1 with a glass tube reactor (length 14 cm, volume 35 cm^3) equipped with an internal guide tube for a thermocouple inside the catalyst bed. The reactor was placed in an

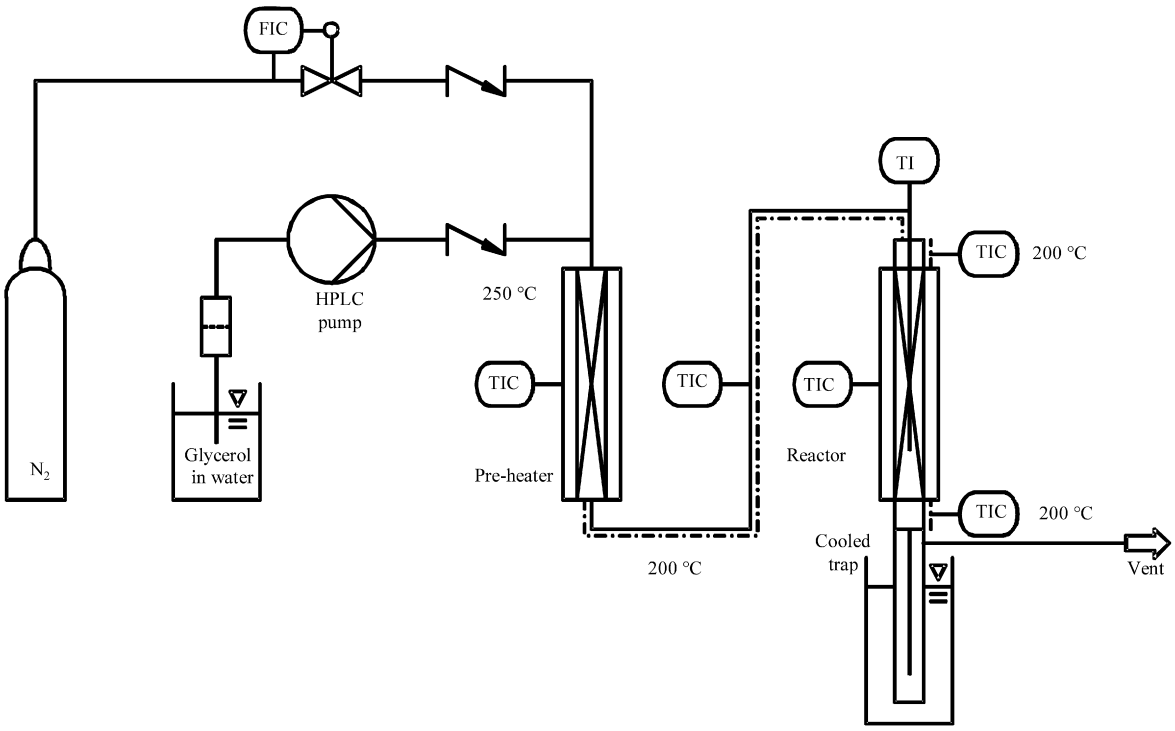

Fig. 1. Flow scheme of continuous bench scale set-up.

electrically heated furnace with an internal diameter matching the outer diameter of the reactor to optimise heat transfer and temperature profile. The particle size of the solids tested was in the range from 315 to 500 μm. Besides the prepared supported catalysts, bulk heteropolyacids as well as pure supports with same particle size were tested. Usually the catalyst was diluted with inert quartz by a factor of ca. 20 to avoid hot spots. Measurement of the axial temperature profile in the catalyst bed proofed that the reaction was carried out at isothermal conditions. All reactant and product containing tubes were heated to at least 200 °C to avoid condensation, and these set-points were validated by measuring the internal temperature in the tubes. A HPLC pump (*Gilson*) was used to feed a mixture of glycerol (analytical grade) and water (10% glycerol by weight) into the flow plant. Nitrogen served as dilutant and the flow rate was adjusted with a mass flow controller (*Bronkhorst*). The feed was first evaporated in a preheater (250 °C) and then entered the reactor in downflow mode. Products were collected first in a cold trap (0 °C) that was connected directly to the reactor outlet. The mass balance for each trap was determined to check proper operation of the set-up and the collected liquids were analysed offline by means of GC. Volatile compounds that were not retained in the cold trap were conducted through a gas-collecting cylinder and also analysed by offline GC. Gas phase analysis allowed quantification of permanent gases, volatile hydrocarbons and volatile oxygenates.

After setting new reaction parameters, the system was run for at least 1 h to establish steady-state operation. For each set-point, usually two independent samples were collected in cold traps. At the same time, also the corresponding gas samples were collected at the outlet of the traps. The standard test program for each catalyst comprised four consecutive temperature set-points at 225, 250, 275, and 300 °C. All other parameters like catalyst mass (300 mg), feed composition (glycerol mass concentration 10% by weight), and flow rate (0.028 ml/min of aqueous feed, 30 ml/min of nitrogen) were kept constant.

2.4. Analytical methods and evaluation of results

The cold trap contained a measured amount of water to improve absorption of low-boiling compounds and some hydroquinone was added to avoid polymerisation of acrolein. The aqueous samples were analysed without preliminary extraction or separation of water using a gas chromatograph (*Shimadzu GC 17A*) with autosampler equipped with a capillary column (*Chrompack FFAP* 30 m × 0.30 mm × 0.2 μm) and flame ionisation detector (FID, temperature program: 40 °C (4 min)–20 K/min–200 °C (23 min); carrier gas He; 1 μl injection volume; split ratio 80). Quantification was realised with 5% by weight of 1-butanol in water as internal standard by mixing 1000 μl of non-diluted sample and 200 μl of internal standard. Authentic compounds were used for product calibration (acrolein and C_1–C_3 oxygenates).

Gaseous samples were analysed with two separate gas chromatographs (*Shimadzu GC 17A*). The content of the gas collecting cylinder was flushed into a 6-port sampling valve and after injection the permanent gases were eluted with argon as carrier gas on a combination of two packed columns (*PoraPak N*, 3 m × 1/8″; *Molsieve 13X*, 3 m × 1/8″) and analysed by thermal conductivity detector (TCD, temperature program: 40 °C–10 K/min–80 °C–40 K/min–120 °C). The second GC was equipped with a 10-port sampling valve and two parallel analytical lines with He as carrier gas and FID (temperature program: 50 °C–35 K/min–200 °C). One line used a *FFAP capillary column* (50 m × 0.32 mm × 0.2 μm) for analysis of volatile oxygenates. The second line used an *Alumina PLOT column* (25 m × 0.32 mm) for analysis of volatile hydrocarbons.

A total organic carbon (TOC) analyser (*Shimadzu VCPN*) served for quantification of total carbon content (organic and inorganic carbon) in the liquid samples to crosscheck GC analyses.

The contributions of all GC analyses for liquid and gaseous phase were joined to evaluate carbon as well as gas balance. Molar streams for all reactants were calculated from concentration in cold trap, dilution, and sampling time. Calculation of glycerol con-

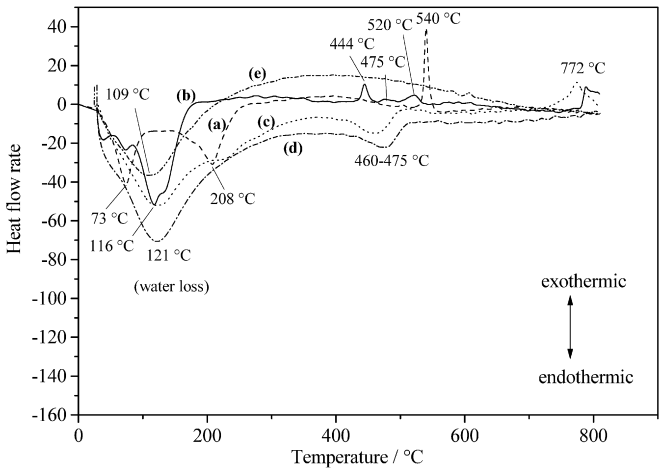

Fig. 2. DTA plots for non-supported and alumina-supported heteropolyacids: (a) HSiW, (b) HPMo, (c) HPMo20/A5, (d) HSiW20/A5, (e) A5 (heating rate 10 K/min, airflow 1 l/h, 5–20 mg of catalyst).

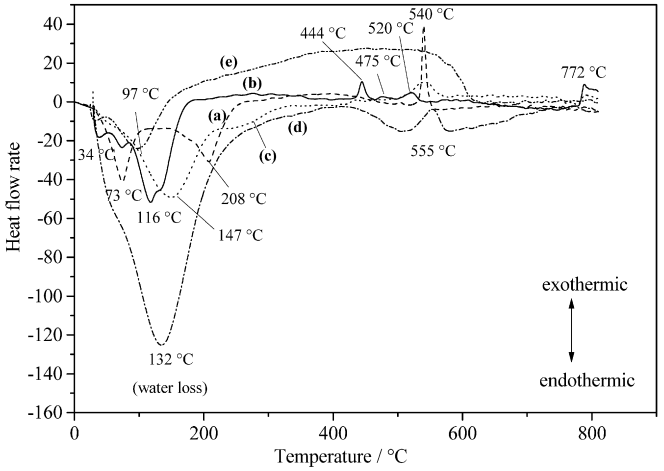

Fig. 3. DTA plots for non-supported and silica-supported heteropolyacids: (a) HSiW, (b) HPMo, (c) HPMo20/S2, (d) HSiW20/S2, (e) S2 (heating rate 10 K/min, airflow 1 l/h, 5–20 mg of catalyst).

version (X_{glycerol}) based on the molar streams of glycerol at the inlet and outlet of the setup as follows:

$$X_{\text{glycerol}} = \frac{\dot{n}_{\text{glycerol,in}} - \dot{n}_{\text{glycerol,out}}}{\dot{n}_{\text{glycerol,in}}} \times 100\%.$$

The selectivities for the products (S_i) were calculated from the molar streams of product and converted feed according to

$$S_i = \frac{\dot{n}_i}{\dot{n}_{\text{Feed},0} - \dot{n}_{\text{Feed}}} \times \frac{z_i}{z_{\text{Feed}}} \times 100\%,$$

where z represents the number of carbon atoms in product i and in the feed molecule (glycerol). The discussed selectivities are therefore carbon-based numbers. Carbon balance is evaluated from non-converted glycerol and yields of identified and calibrated products, therefore carbon balance does not equate to 100%. More details on product identification are given in Section 3.6.

3. Results and discussion

3.1. Differential thermal analysis (DTA)

DTA served to evaluate the thermal stability of the prepared supported catalysts within the target temperature range of 200–350 °C for catalytic tests. The temperatures for thermal decomposition of bulk HPMo, NH_4PMo, HSiW and HPW reported in literature are 375, 400, 445 and 465 °C, respectively [21]. Figs. 2–4 show the DTA curves for alumina-, silica-, and aluminosilicate-supported heteropolyacids, including reference data for bulk heteropolyacids and pure supports.

The DTA curves shown in Figs. 2 and 3 for alumina (A5) and silica (S2) supports gave one endothermic peak at 109 and 97 °C for each support. These peaks are due to physisorbed water.

The DTA curve (Fig. 2) for the bulk phosphomolybdic acid shows three endothermic peaks near 40, 73 and 116 °C, which are accompanied by a considerable weight loss caused by loss of water of crystallisation [22,23]. No weight changes or thermal effects were observed in the temperature range from 150 to 350 °C. Hodnett and Moffat found that at higher temperature (≈400 °C) water is formed from acidic protons and oxygen belonging to the Keggin units [23]. This type of the so-called constitutional water amounts to ≈1.5 moles per Keggin unit. Maksimovskaya and Bondareva found the formation of the so-called anhydride 1 ($HPMo_{12}O_{39}$) at 380 °C due to such loss of the constitutional water [24]. Rocchiccioli-Deltcheff et al. carried out Raman investigations after thermal treatment up to 380 °C and observed

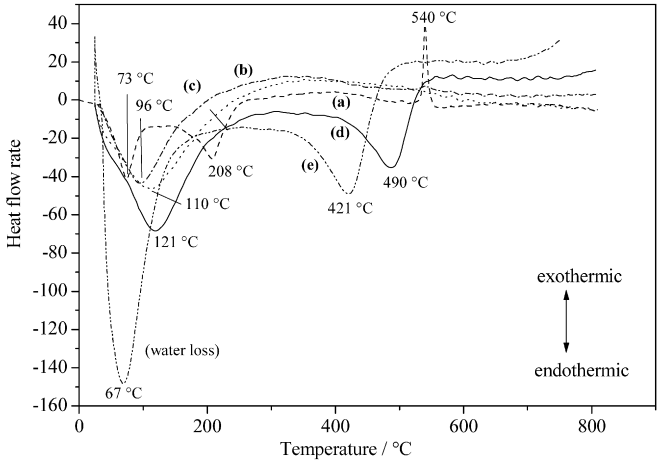

Fig. 4. DTA plots for HSiW supported on different supports: (a) HSiW, (b) HSiW20/S11, (c) HSiW20/A12, (d) HSiW20/AS4, (e) AS4 (heating rate 10 K/min, airflow 1 l/h).

a small modification in the band around 900 cm^{-1}. This region is cited for the stretching vibration (υ_{as} Mo–O_b–Mo) that is sensitive for dehydration process induced by thermal treatment [25]. Maksimovskaya et al. reported that near 400 °C $HPMo_{12}O_{39}$ transforms into MoO_2HPO_4 and MoO_3 or $[PMo_{12}O_{38}][PMo_{12}O_{39}]$ (so-called anhydride 2) [26]. The formed molybdenum oxide is being assigned to β-MoO_3 [25]. Therefore, the exothermic peak for bulk phosphomolybdic acid at 444 °C might be due to the crystallisation of β-MoO_3. Above 450 °C anhydride 2 decomposes to yield $(MoO_2)_2(P_2O_7)$ and α-MoO_3 [25], corresponding to the broad exothermic peak at 475 °C. The exothermic peak at 520 °C is due to the crystallisation of the resulting α-MoO_3 [25].

The DTA for bulk silicotungstic acid displays two endothermic peaks at 73 and 208 °C (Fig. 2); the first peak is due to the loss of physisorbed water, while the second endothermic peak is due to the removal of water from this hydrated heteropolyacid [27]. Babad-Zakhryapin and Moiseev claimed that the removal of water from this hydrate gives an endothermic effect within this temperature region (200–285 °C) [28]. However, no important structural changes are observed in this temperature region. Anhydrous 12-silicotungstic acid is intact up to 400 °C [29]. The exothermic peak at 540 °C is due to crystallisation of a new compound. This compound is assigned to WO_3(Si) that could be considered as a solid solution of silicon in tungsten trioxide [30].

Similar to the bulk materials, the DTA plots for the alumina-supported catalysts HSiW20/A5 and HPMo20/A5 show an endothermic peak due to loss of water (ca. 120 °C) accompanied by a weight loss in TGA (Fig. 2). These samples show an additional endothermic peak in a very narrow range of 460 to 475 °C independent of the heteropolyacid compound and no appreciable weight change at temperatures up to 800 °C is noticed. The same behaviour was observed for supported heteropolyacids with 10% loading. The appearance of the second endothermic peak might be due to interaction between the support alumina and heteropolyacid.

All silica-supported samples show endothermic peaks around 132 °C due to loss of water (Fig. 3). In contrast to the alumina-supported samples, an exothermic peak appears in the range from 475 to 557 °C that indicates the decomposition of the Keggin anion. These peaks are broader and one can conclude that these data mainly represent the influence of the thermal stability of different heteropolyacids as they interact with the support weakly. It is confirmed by literature data that bulk HPW and HSiW heteropolyacids are more stable than HPMo and NH_4PMo. Immobilisation on silica obviously increases the thermal stability of the Keggin structures in comparison with their parent bulk heteropolyacids. Silica is a well-suited support for HPA if compared to alumina [21,31–33]. On the other hand, some research groups derived contradictory conclusions for heteropolyacid stability over silica [34,35].

Alumina seems to interact more strongly with the active compounds than silica does. This interaction could be explained as follows: when the solution and the support are in contact, the surface hydroxyl groups of Al_2O_3 become protonated, yielding MOH_2^+ (M is the metal ion). As a result, the surface gets a positive charge that can interact strongly with heteropolyanion $(HPAn)^{-1}$ forming M(HPAn) [36] that is being distorted. In this case, the HPA would obviously loose acidity. Silanol OH groups may similarly participate in HPA bonding to form $(SiOH_2^+)(HPAn)^{-1}$. In dependence on the nature of the support such interaction leads to the formation of active intermediates with different strength of Brønsted acid sites and stabilised structures. As a result, two effects may get compensated: On silica, due to weak interaction mainly exothermic decomposition of HPA accompanied by loss of constitutional water is observed, whereas on alumina an additional stabilisation effect due to stronger interaction between support and HPA occurs. This interaction has to be resolved before thermal destruction of the HPA occurs. If the first thermal effect is larger than the second one, the overall effect will be inverted and endothermic peaks should be observable. However, the structure of all supported HPAs seems to be maintained at least up to 400 °C, and hence this temperature should be suitable for calcination of the catalyst precursors at least.

Fig. 4 shows DTA curves for catalysts with 20% HSiW supported on alumina (pore diameter 12 nm), silica (11 nm) and aluminosilicate (4 nm) as well as for the bulk HSiW and support AS4. They reveal a single endothermic peak in the range from 73 to 116 °C due to loss of water. The aluminosilicate-supported catalyst possesses two endothermic peaks at 121 °C and 490 °C for loss of water and the interaction between hydroxyl groups of aluminosilicate and the heteropolyanion.

3.2. Nitrogen adsorption

Textural properties (BET surface area, pore volume and average pore diameter) for heteropolyacids immobilised on five different supports derived from nitrogen physisorption isotherms are given in Table 1. The specific BET surface areas for various heteropolyacids supported on alumina (A5) with 20% loading reached 249–270 m^2/g. The silica-supported heteropolyacids with 20% loading had surface areas from 418 to 487 m^2/g. Additionally, immobilising silicotungstic acid on A12, S11 and AS4 resulted in materials with surface areas of 250, 259 and 309 m^2/g, respectively.

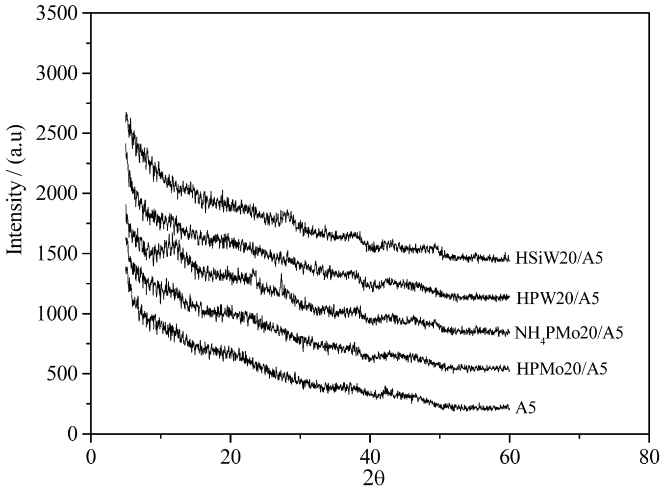

Fig. 5. X-ray diffractograms for alumina-supported heteropolyacids.

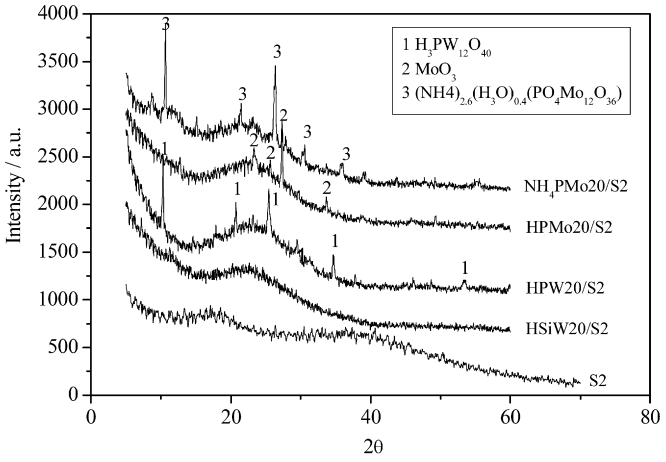

Fig. 6. X-ray diffractograms for silica-supported heteropolyacids.

Lowering the loading of heteropolyacid from 20 to 10 wt% always led to increased surface area. This effect seems to be stronger on silica than on alumina or aluminosilicate. The decrease in the surface area may be attributed to wet impregnation method. The data in Table 1 show that the silica-supported catalysts loose about one third of their initial specific surface area during impregnation. This is understandable when looking at the pore volume and in particular at the average diameter of pores: the pores for the alumina are more than double in size compared to silica containing materials. The latter contain more micropores, and first many of them were plugged with the heteropolyacids as the Keggin units are small enough (diameter ≈ 1.2 nm) to enter even micropores [37].

3.3. X-ray diffraction (XRD)

The most intensive reflections for bulk heteropolyacids NH_4PMo, HPMo, HSiW, HPW are expected at $2\theta = 26.5$, 27.3, 8.0, and 10.3, respectively. However, for alumina-supported heteropolyacids, the reflections detected neither correspond to the heteropolyacids nor to other crystalline phases even at a loading of 20% by weight and hence the samples are completely X-ray amorphous (Fig. 5).

On the other hand, most of the diffractograms for heteropolyacids supported on silica S2 exhibit definite peaks (Fig. 6). NH_4PMo20/S2 shows reflections at $2\theta = 26.4$ and 10.7 that can

be assigned to the Keggin-type structure of $(NH_4)_{2.6}(H_3O)_{0.4}$-$(PO_4Mo_{12}O_{36})$ (PDF 70-129). For HPMo20/S2, signals at $2\theta = 27.3$ and 23.3 indicate the presence of MoO_3 phase (PDF 89-7112). The formation of anhydrous heteropolyanion occurs in the temperature region up to 350 °C. Then, the loss of constitutional water starts up to ca. 435 °C. The HPA decomposes into mainly β-MoO_3 with small portion of α-MoO_3. During heating to 500 °C only α-MoO_3 can be observed [38]. Reflections of β-MoO_3 and some of α-MoO_3 are clearly to see in the pattern of HPMo at 350 °C [38].

In the diffractogram for HPW20/S2 the signals at $2\theta = 10.3$ and 25.3 belong to the Keggin-type $H_3PW_{12}O_{40}$ phase (PDF 75-2125). These data prove that molybdenum-containing heteropolyacids are the least stable compounds in this group in coincidence with results from thermal analysis. As an exception, HSiW20/S2 shows no reflections in the diffractogram at all, indicating that HSiW has been dispersed even over the silica support in the same manner as observed with alumina support (see below).

The diffractograms for silicotungstic acid (HSiW20) supported on alumina A12, silica S11 and aluminosilicate AS4 are not meaningful. HSiW20/S11 and HSiW20/A12 samples are X-ray amorphous and show no crystalline phase. On the other hand, non-calcined HSiW20/AS4 showed three humps at $2\theta = 28.2$, 38.6, and 49.2 that were assigned to $Al_2O_3{\cdot}H_2O$ (boehmite). After calcination at 400 °C, the intensity of these humps significantly decreases maybe due to dehydroxylation as inferred from the endothermic peak in DTA. Based on the size of the Keggin anion (diameter $\approx$ 1.2 nm) and the available surface area of alumina A5 and aluminosilicate AS4 (298 and 384 m^2/g), theoretically a loading of about 80% of HPA would saturate the surface. Therefore, 20% loading may lead to species that either are highly dispersed or decomposed on the surface. Kozhevnikov found that at higher loadings, 30–50% of HPA is present as crystalline phase on silica with 200–300 m^2/g but at low loadings mainly fine dispersed species are formed. Obviously, X-ray detectable HPA crystal phase is developed on silica surface only above 20% loading [21]. High concentration of the active phase saturates the support surface and then some HPA molecules could not access the support mesopores and crystallise as separate phase that could be detected by XRD.

The surface coverage of HSiW on HSiW20/A5, HSiW20/A12, HSiW20/S2, HSiW20/S11, HSiW20/AS4 was calculated according to a literature method using the following equation: $0.2/(0.8 \times M_{SiW} \times S_{BET})$, where M_{SiW} is the molecular weight of SiW (=3310.66 g/mol) loaded on the silica and S_{BET} is the surface area of the support, respectively [20]. The calculated surface density values were 0.254 (HSiW20/A5), 0.258 (HSiW20/A12), 0.120 (HSiW20/S2), 0.235 (HSiW20/S11) and 0.197 (HSiW20/AS4) $\mu mol/m^2$, respectively. The low value for HSiW20/S2 indicates higher dispersion over the silica and this could explain why only HSiW20/S2 did not show any XRD pattern. As seen from the previous equation, surface density is inversely proportional to the molecular weight of the HPA. Thus, as HSiW has higher molecular weight compared with HPMo, silicotungstic acid would be more dispersed over silica support as found by the XRD studies and this could explain why HPMo and HPW showed reflections while HSiW did not.

From these studies, it can be concluded that the interaction of the heteropolyacids is much stronger with alumina than with silica. A more reasonable explanation refers to the surface zeta potential of the supports than aforementioned hydrogen bonds. Alumina has a typical isoelectric point around pH 10 and silica around pH 2 [39]. As discussed above, at the preparation conditions in aqueous phase, alumina should be positively charged and therefore strong interaction with the negatively charged heteropolyanions is possible. Silica surface is negatively charged and hence the heteropolyanions rather tend to agglomerate. If this happens, the heteropolyacids can form X-ray detectable crystallites.

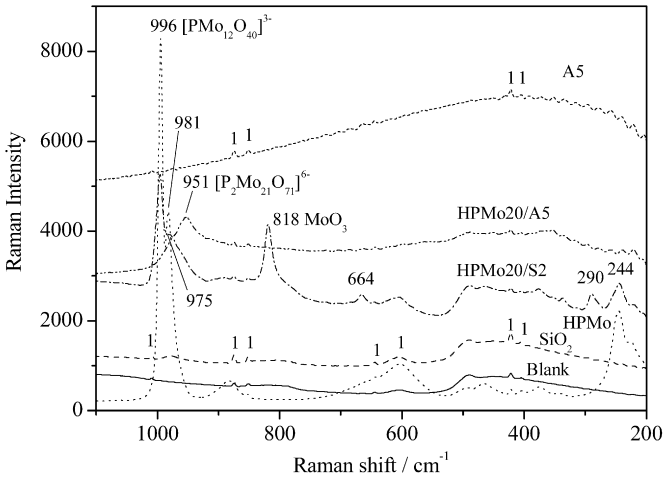

Fig. 7. Raman spectra for HPMo supported over alumina and silica (1 = bands from glass tube).

However, alumina-supported samples are always found to be X-ray amorphous.

3.4. Raman spectroscopy

Raman technique is known to be well suited for observation of Keggin structures [40] to prove the presence of HPA structures. Fig. 7 represents Raman spectra for HPMo20/A5 and HPMo20/S2. The Raman spectrum for bulk HPMo gives bands at 996, 983, 882, 603, and 246 cm^{-1} which are assigned to symmetric (υ_s) and asymmetric (υ_{as}) vibrations of terminal oxygen υ_s(Mo–O_t) and υ_{as}(Mo–O_t), of corner shared bridged oxygen υ_s(Mo–O_b–Mo), of edge shared bridged oxygen υ_s(Mo–O_c–Mo) and of oxygen in the central tetrahedron υ_s(Mo–O_a) [38]. Comparing the Raman spectrum of HPMo20/S2 with bulk HPMo spectrum reveals bands at 996, 981, 975, 818, 606 and 243 cm^{-1} that were assigned to Keggin heteropolyanion $(PMo_{12}O_{40})^{3-}$ except the band at 818 cm^{-1} that is assigned to MoO_3 formed by partly degradation of HPMo [38]. For HPMo20/A5, a broad band at 951 cm^{-1} is detected, which is related to the stretching vibrations of υ_s(Mo–O_b–Mo) groups and is influenced by hydrolysis/dehydration processes [38,41]. Some NMR studies could support these findings. Vázquez et al. [42] reported in their studies on HPMo supported over alumina two lines present at −3.25 and −10.76 ppm. The first chemical shift is assigned to the Keggin unit and the second could not be strictly assigned but probably it may be related to the strong HPMo interaction with OH groups of alumina support. A similar shift (−10.76 ppm) was observed by Rao et al. [32] that was assigned may be due to HPMo interacting with the support surface or partially reduced HPMo [43] or unidentified species. These species might be dimeric $[P_2Mo_{21}O_{71}]^{6-}$ resembling to $[P_2W_{21}O_{71}]^{6-}$ that are formed by partial transformation of $[PW_{12}O_{40}]^{3-}$ supported on alumina [44].

Fig. 8 illustrates that the most intense bands in bulk HSiW appear at 998 cm^{-1} (stretching of W=O), 974 cm^{-1} (bending of W–O_c–W), and 555 cm^{-1} (bending of O–Si–O). The signals at 329 and 227 cm^{-1} are assigned to WO_3, but could also stem from impurities. The spectrum of HSiW20/S2 shows peaks at 998 cm^{-1} and 970 cm^{-1} for the W=O stretching and W–O–W bending mode, indicating the preservation of the Keggin structure in the HSiW on the surface of silica. The use of alumina as support for the same heteropolyacid in HSiW20/A5 leads to a shift in W–O–W bending mode to 962 cm^{-1}. Such a distortion effect within the Keggin structure could evidence a strong interaction of HSiW with alumina surface.

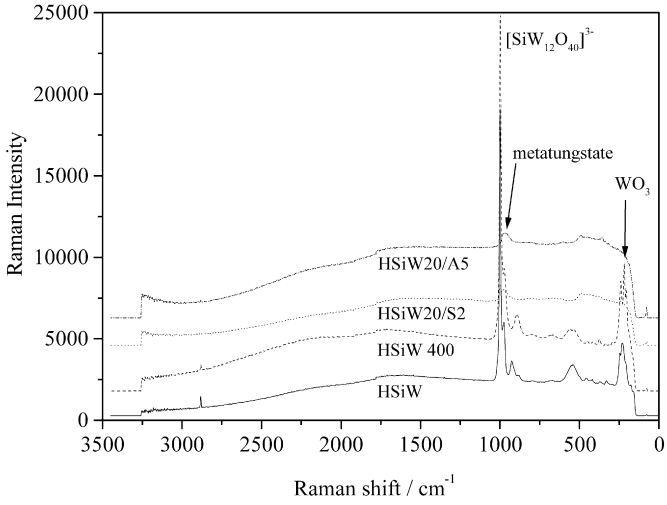

Fig. 8. Raman spectra for bulk HSiW and HSiW supported on alumina and silica (oven dried samples; HSiW400 = calcined at 400 °C).

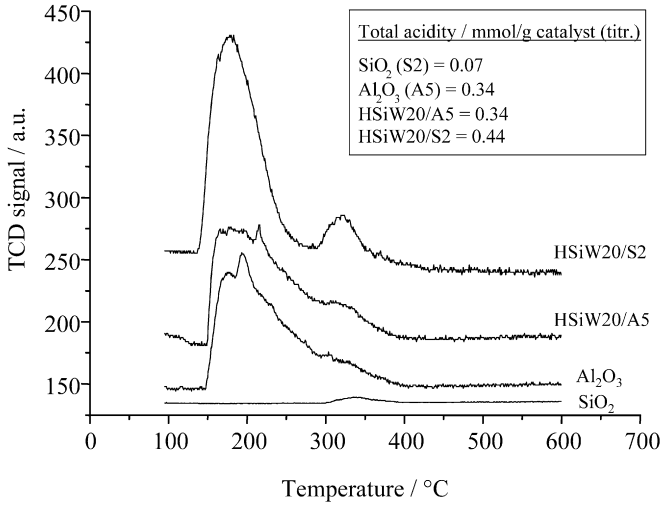

Fig. 9. Profiles for TPD of ammonia for supports silica S2 and alumina A5 and catalysts HSiW20/A5 and HSiW20/S2.

3.5. Temperature programmed desorption of ammonia (TPDA)

Alumina support A5 calcined at 400 °C shows much higher total acidity from titration (0.34 mmol NH_3/g) than silica (0.07 mmol/g), as expected (Fig. 9). The maxima for ammonia desorption from alumina and silica supports were observed at temperatures of approximately 180 and 320 °C, respectively. A small additional peak around 195 °C is detected for alumina. The classification of strength of acid sites is weak (150–300 °C), medium (300–500 °C), and strong (500–650 °C) [45].

Modification of the supports with HPA seems to induce new medium acidic sites at least. After impregnating the supports with HSiW, the overall acidity measured by titration of HSiW20/A5 stays unchanged (0.34 mmol/g), whereas the amount of adsorbed ammonia rises from 0.07 to 0.44 mmol/g for the HSiW20/S2 catalyst. The TPDA profile of HSiW20/A5 shows three peaks appearing at approximately 180, 215 and 310 °C. The TPDA curve of HSiW20/S2 reveals only two peaks at 180 and 320 °C. The pure alumina support shows much more total acidity compared to the silica, therefore, the HPA anion is expected to interact to a large extent. In this case, a portion of the HPA would loose its acidity due to the distortion of the Keggin structure. The addition of heteropolyacid did not introduce any new sites, but led to a replacement by other acidic sites. On the other hand, the overall acidity of the silica surface significantly increased after impregnation with heteropolyacid as the amount of acidic sites over silica is larger compared to alumina-supported sample. The weak interaction of silica with the HPA keeps its Brønsted acid character and leads to an increased proportion of medium acid sites. Desorption peaks above 400 °C in the TPDA curves (registered by TCD) of the supported HPAs may point to their destruction.

3.6. Product identification

Product analyses were carried out as mentioned above by using several GC units. Acrolein is always the predominant product in both liquid and gaseous phase besides some by-products in different quantities (acetaldehyde, propionaldehyde, acetone, methanol, ethanol, allyl alcohol, hydroxyacetone, acetic acid, 1,2-propandiol, and propionic acid). Some minor by-products were not identified. However, a defined portion of acrolein, acetaldehyde and propionaldehyde escaped from the cold trap but were quantified from the product gas in addition to liquid phase. Absence of O_2 validated proper sampling and the absence of CO and CO_2 indicated that reforming of glycerol did not occur. Routinely evaluated mass balances for each cold trap accounted for 92–98% (without gaseous compounds). Carbon balances were calculated from detected products in gas and liquid phase for each set-point and added up to 60–95% (values can be calculated from Table 2). Missing carbon is due to (i) some unknown minor peaks in chromatograms and (ii) mostly deposits on the catalyst surface depending on the reaction conditions (glycerol oligomers, polymers from acrolein, etc.) as also indicated by GC–MS after extraction spent catalyst samples. Carbonaceous deposits on the spent catalyst are not included in carbon balance due to uncertain quantification. Casually made TOC analyses of carbon content in liquid samples revealed good agreement with GC data.

3.7. Influence of temperature on conversion and selectivity

The catalytic tests with the pure heteropolyacids in the temperature range from 225 to 300 °C showed that HSiW was the most active solid reaching 63% conversion at 275 °C. No catalyst revealed complete conversion. HPMo deactivated rapidly and HPW and NH_4PMo showed a moderate increase in conversion with temperature. There was no general trend observable for the four heteropolyacids and maximum selectivity for acrolein never exceeded 50%.

The tests with the silica-supported heteropolyacids showed that these materials rapidly deactivate after few hours. The deactivation could occur due to decomposition of the HPA active compound or blocking of the catalyst surface by carbonaceous deposits (see below). Activity of the silica-supported heteropolyacids decreases in the order HSiW20/S2 > HPW20/S2 > NH_4PMo20/S2 > HPMo20/S2. Data for these catalysts are listed in Table 2. Increasing the pore size of the support (from 2 to 11 nm) enhances the catalytic activity and hence the conversion is complete for HSiW20/S11 at 275 °C. Nevertheless, rapid deactivation was observed in the test with the latter material.

Fig. 10 shows conversion with increase in temperature for HSiW20/A5, HPMo20/A5, HSiW20/A12, as well as for the pure supports A5 and A12. In contrast to bulk and silica-supported catalysts, all heteropolyacids supported on alumina A5 as well as pure alumina A5 itself show a consistent increase in glycerol conversion. No such heavy deactivation was observed as for silica-supported samples. The surface specific rate of acrolein formation on alumina-supported catalysts is approximately one order of magnitude higher than for silica-supported samples (Table 2). At the

Table 2
Results from glycerol dehydration with alumina (A5)- and silica (S2)-supported catalysts

T [°C]	X [%]	Y (known products) [%]	Rate of acrolein formation [μmol/(m^2 h)]	S (individual products)					
				Acetone [%]	Acrolein [%]	Ethanol [%]	Allyl alcohol [%]	Hydroxyacetone [%]	Total [%]
				HPMo20/A5					
225	60.5	21.2	0.15	8.8	10.6	3.8	6.7	3.0	35.0
250	83.5	42.5	0.38	8.5	19.1	4.0	6.9	6.4	50.9
275	97.3	86.9	1.04	6.5	45.0	2.3	8.2	10.9	89.3
300	98.0	84.7	1.04	7.2	43.8	2.4	6.4	5.2	85.1
				NH_4PMo20/A5					
225	47.6	17.2	0.15	7.0	14.3	4.4	4.1	3.3	36.2
250	71.5	40.6	0.43	4.5	27.1	2.7	7.5	6.7	56.8
275	95.6	66.3	0.79	4.4	37.1	2.2	7.0	6.4	69.4
300	99.6	50.4	0.33	2.5	14.9	2.8	5.1	4.4	50.6
				HPW20/A5					
225	17.3	16.8	0.08	40.3	19.8	22.1	0.6	5.2	96.9
250	72.7	37.5	0.38	15.2	23.5	3.7	0.8	4.2	51.5
275	99.2	76.8	1.14	4.3	51.7	2.4	1.8	8.0	77.4
300	97.4	58.9	0.47	4.4	21.7	3.5	1.4	6.1	60.5
				HSiW20/A5					
225	22.9	4.9	0.08	2.7	14.3	0	0	0	21.5
250	74.2	26.3	0.49	1.2	27.4	0.5	0.6	3.2	35.4
275	98.4	83.9	1.50	2.6	63.6	1.6	1.5	7.9	85.3
300	99.5	83.1	1.41	2.0	58.9	1.2	1.2	4.3	83.5
				HPMo20/S2					
225	47.0	10.4	0.03	7.1	4.3	6.1	1.7	1.1	22.1
250	21.8	14.2	0.07	12.2	23.9	8.6	8.0	5.6	65.0
275	8.9	6.6	0.03	14.0	27.8	8.9	5.9	7.8	73.7
300	55.7	21.5	0.15	1.7	19.8	1.3	3.8	5.5	38.6
				NH_4PMo20/S2					
225	43.8	12.2	0.04	10.5	7.4	5.7	1.5	1.2	27.8
250	34.1	21.1	0.09	18.8	20.8	10.0	4.3	3.3	62.2
275	48.9	29.7	0.15	10.7	24.4	5.7	7.0	5.2	60.7
300	70.7	40.1	0.19	5.5	22.3	2.6	8.7	6.6	56.7
				HPW20/S2					
225	83.6	26.6	0.22	5.4	21.6	2.8	0.1	0.7	31.8
250	52.9	21.5	0.19	5.4	29.9	2.6	0.1	1.1	40.5
275	55.5	23.9	0.19	6.6	28.0	3.4	0.2	2.0	43.2
300	67.1	27.6	0.24	3.0	29.1	1.4	0.4	3.0	41.1
				HSiW20/S2					
225	65.1	5.4	0.05	1.4	5.0	0.9	0.2	0.3	8.2
250	70.0	11.9	0.13	1.2	12.7	1.2	0.1	0.8	16.9
275	79.2	23.8	0.24	3.3	21.0	2.5	0.1	1.4	30.0
300	64.8	36	0.36	3.3	39.0	2.1	0.3	4.4	36.0

Note. Catalyst mass = 300 mg, glycerol mass concentration = 10 wt%, flow rate (liquid) = 0.028 ml/min, 30 ml/min of nitrogen, T = reaction temperature, X = conversion, Y = yield, S = selectivity.

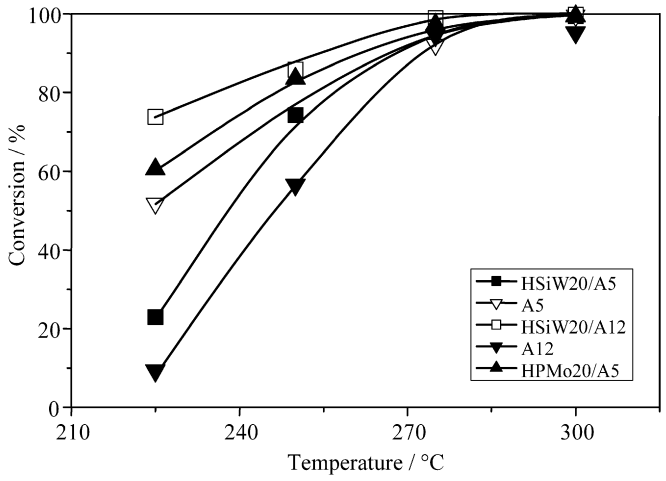

Fig. 10. Influence of temperature on glycerol conversion for alumina and alumina-supported heteropolyacids (10% of glycerol in water, $W/F = 0.15$ kg h mol^{-1}).

chosen modified contact time of 0.15 kg h mol^{-1}, with most catalysts complete conversion was obtained near 275 °C. Comparison of HSiW20/A5 with HSiW20/A12 shows that increasing the support pore size enhances the catalytic activity as already observed for silica-supported catalysts. HSiW20/AS4 catalyst shows similar performance as alumina-supported catalysts, reaching maximum conversion at 275 °C without noticeable deactivation at higher temperature, too. Based on these results, it can be concluded that the nature of the carrier has a significant influence on the catalyst activity and its lifetime.

Considering the supports, the catalyst activity as well as lifetime seem to decrease in the order alumina ⩾ aluminosilicates > silica. At the same time, the results also demonstrate that impregnation of all kinds of heteropolyacids onto supports leads to a significantly increased performance compared to bulk heteropolyacids. Supporting heteropolyacids causes the dispersion of HPA as found by XRD, in particular for alumina-supported samples. The dispersion leads to an increase in the total amount of catalytically active protons. The use of these dispersed catalysts permits a better accessibility of glycerol molecules to active sites and thus high conversions can be obtained. In view of this, HSiW20/A5 showed

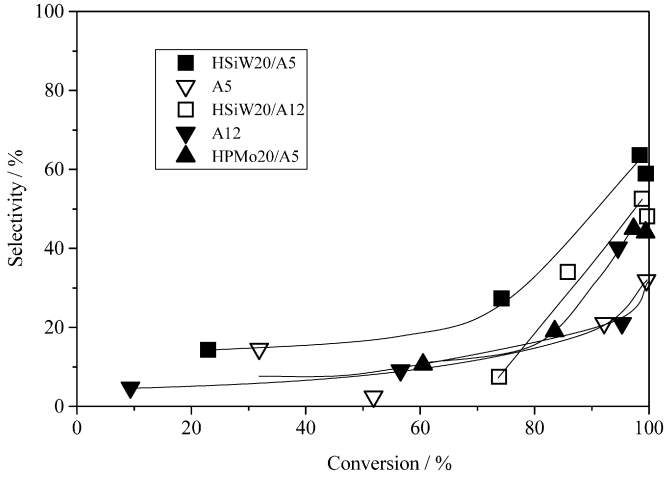

Fig. 11. Acrolein selectivity versus conversion over alumina supports and alumina–supported HPAs (10% of glycerol in water, $W/F = 0.15$ kg h mol^{-1}).

higher activity than HSiW20/S2 (see also Table 2). However, the effect of changing the HPA mass fraction on the described supports from 10 to 20% on catalytic conversion seems to be negligible. This observation is valid for alumina as well as silica-supported samples.

The most prominent benefit of using these supports rises from the significant impact on product distribution. With catalysts supported on silica S2 (pore diameter 2 nm), the plots of selectivity versus glycerol conversion did not lead to reasonable results due to the rapid deactivation, probably sampling in shorter time distances could give more reliable data but this could not be realised due to the given sampling procedure (time interval of ca. 1 h used). Nevertheless, some of these data are listed in Table 2, too. HSiW as active compound is superior to the other S2-supported catalysts with regard to acrolein formation. A maximum selectivity for acrolein of 39% at 63% glycerol conversion was achieved for HSiW20/S2. Usage of HSiW20/S11-supported catalyst boosts the acrolein yield dramatically as selectivity rises to 73% at 67% conversion.

The pure alumina supports A5 and A12 themselves showed a considerably high catalytic activity in the studied reaction, probably due to their acidic properties. However, the selectivity for acrolein on these materials (A5: 30% at complete conversion; A12: 40% at 93% conversion) was significantly less than for supported HPA (Fig. 11). Among the four catalysts supported on alumina with 5 nm pore diameter, HSiW20/A5 was the most selective catalyst as it gives 64% selectivity for acrolein at complete conversion at 275 °C. To simplify the diagram only data for selected catalysts were plotted. Changing the pore size from 5 to 12 nm further enhances the selectivity of acrolein formation. In general, the selectivity for acrolein increases with glycerol conversion and contact time, respectively. This clearly indicates a consecutive reaction pathway.

HSiW on aluminosilicate leads to high acrolein selectivity of 67% at nearly complete conversion similar to the alumina-supported heteropolyacids. As observed for all other catalysts, the maximum selectivity is obtained at 275 °C that seems to be indeed an optimum temperature with regard to acrolein formation.

In comparison to all other tested heteropolyacids, HSiW always led to the highest acrolein selectivity whether it was used as bulk material or impregnated onto supports. The outstanding performance of HSiW is linked to high acidity and hydrolytic stability even in aqueous environment without forming acetals [21]. Verhoef et al. reported that supported silicotungstic acid is more active than tungstophosphoric acid in esterification reactions due to the presence of higher number of Keggin protons of HSiW (four) as compared to HPW or HPMo (three) [46]. Varisli et al. found that HSiW is more stable than HPW at temperatures higher than 200 °C in dehydration of ethanol [47]. On the other hand, phosphomolybdic compounds always showed the lowest selectivity for acrolein whereas selectivity for acetaldehyde, propionaldehyde, acetone, and acetic acid increased. These results might be due to the redox properties introduced by molybdenum that enables additional reaction pathways at the cost of acrolein formation [20].

Furthermore, it seems that pores larger than 4 nm lead to more effective catalysts because they provide sufficient space for Keggin units on the inner surface and their interaction with adsorbed glycerol molecules. If a large proportion of the heteropolyacids was fixed in mesopores (2 to 12 nm in this study), the formation of crystallites with sufficient size to generate XRD pattern could be hindered. This possibly explains the absence of XRD patterns for the alumina containing catalyst that contain a large portion of mesopores. On the other hand, for materials with a large portion of micropores (silica), the heteropolyacid compounds mainly are located on the outer surface and are not restricted in forming crystallites. In addition, the influence of internal mass transfer limitation will be reduced with larger pores [20].

Although heteropolyacids are probably partially decomposed over the alumina surface, they show high catalytic activity and selectivity. Alejandre et al. found that the surface tungsten Lewis acidic centres are more acidic on alumina than on other supports [48]. IR experiments revealed that the presence of such tungsten oxide species induces Brønsted acidity. At catalytic reactions where water vapour is frequently present at relatively high temperature (≈573 K), it probably hydrates a portion of the surface forming Brønsted acidity centres. So the Lewis acidity corresponds to the anhydrous form and Brønsted acidity to the hydrated form. Such hydration could happen to HPMo but due to its low thermal stability and additional redox properties, its catalytic activity is lower than HSiW.

3.8. Influence of contact time on conversion and selectivity over $H_4SiW_{12}O_{40}$

HSiW is the most effective heteropolyacid while alumina and aluminosilicate are superior supports compared to silica in terms of better performance. In order to exploit such potential effects, the influence of combination of these materials on the performance was investigated more in detail by varying the residence time at a constant temperature of 275 °C (Fig. 12). With HSiW20/AS4, HSiW20/A12 and HSiW20/A5 the catalytic activity increases consistently with residence time and complete conversion is reached at approximately 0.2 s (Fig. 12a). Acrolein selectivity on these catalysts seems to pass through a maximum by further increase of residence time (Fig. 12b). This might be due to consecutive reactions like acrolein degradation or polymerisation. A change in the colour of spent catalysts indicated the formation of deposits on the catalyst surface.

The maximum acrolein selectivity reached 74% with HSiW20/AS4 ($X = 99\%$), 71% with HSiW20/A12 ($X = 91\%$) and 51% with HSiW20/A5 ($X = 100\%$). Obviously, HSiW20/AS4 was the best performing catalyst at 275 °C. The data also clearly suggest that increase in the pore size changes the product distribution, improves lifetime and increases acrolein yield. An enlargement of the mean pore diameter of the support alumina from approximately 5 to 12 nm leads to a gain of approximately 20% in acrolein selectivity. Though HSiW20/AS4 has a comparatively low pore diameter of 4 nm, it still keeps its stability and activity. Long-term tests with different alumina and aluminosilicate supports in steam atmosphere at 240 °C revealed an increase in hydrothermal stability for aluminosilicate compared to aluminas [49]. The improved sta-

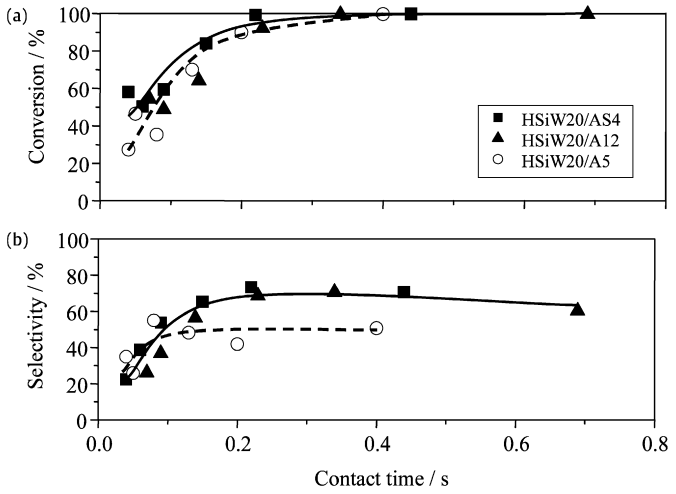

Fig. 12. (a) Conversion and (b) acrolein selectivity versus residence time with HSiW20/A12, HSiW20/A5 and HSiW20/AS4 (275 °C, 0.6 g of catalyst).

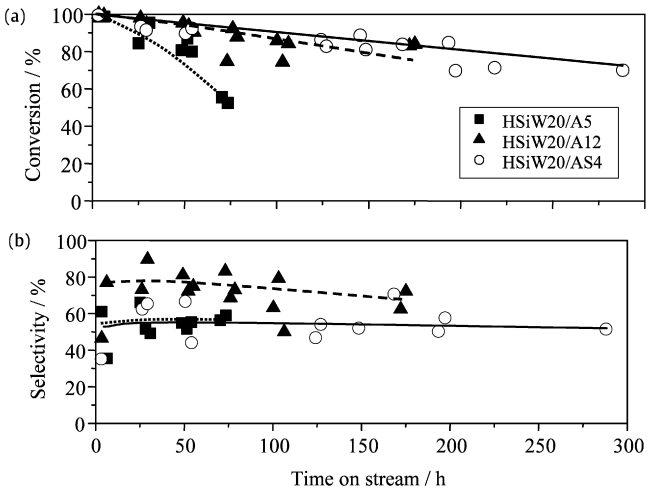

Fig. 13. Long-term runs with HSiW20 supported on different materials. (a) Conversion, (b) acrolein selectivity versus time-on-stream (275 °C, 0.15 kg h mol^{-1}).

bility of the textural properties of aluminosilicates like support AS4 (Siral® 10) may compensate the lower diameter of the pores. Besides that, may be a pore size of 4 nm is some kind of a threshold value as reported by Tsukuda et al. [20], who found that silica with 3 nm was the least active support.

3.9. Long-term stability of $H_4SiW_{12}O_{40}$ catalysts

The above discussed experiments with bulk and silica-supported HPAs at standard reaction conditions under variation of temperature led to rapid deactivation, either due to heavy coking or also probably due to structural changes in the active phase. On the other hand, the alumina- and aluminosilicate-supported samples were apparently stable during these tests. Spent silica-containing samples were deeply black supporting a deactivation by coking, whereas spent alumina- and aluminosilicate-supported catalysts usually changed to slight brown only. This suggests a deactivation mechanism due to the blocking of the solid surface with high-boiling compounds. The oligomerisation of glycerol or non-saturated products like acrolein is a possible route towards such deposits. Both reactions are definitely connected to the catalyst acidity and pore size.

Therefore, alumina- and aluminosilicate-supported HSiW catalyst samples (HSiW20/A5, HSiW20/A12 and HSiW20/AS4) were checked for their long-term performance without interruption to evaluate deactivation. The course of conversion and selectivity is shown in Figs. 13a and 13b. Initial conversion of glycerol with all these catalysts was complete, but decreased rapidly to approximately 50% within 75 h on-stream with HSiW20/A5. Both the other catalysts HSiW20/A12 and HSiW20/AS4 showed significantly higher stability as they lost less than 20% of activity within 200 h. After 300 h on-stream, HSiW20/AS4 still showed a conversion above 70%. At the same time, acrolein selectivity was nearly constant for all the catalysts. Indeed the product distribution did not show any significant change during the complete test. This behaviour points at a deactivation mechanism forming deposits on the surface that reduces the total number of accessible active sites whereas the nature of the active sites that controls the selectivity remains unchanged.

Finally, a regeneration test was carried out with HSiW20/AS4 after conversion decreased from 100 to 75% within 300 h. Nitrogen flow was replaced by a mixture of 99% of N_2 and 1% of O_2 and temperature was raised to 325 °C for 24 h. After switching back to standard reaction conditions, conversion recovered to 100% and acrolein selectivity reached 60%. This demonstrates that recovery of initial catalyst activity is possible easily by in situ oxidative regeneration.

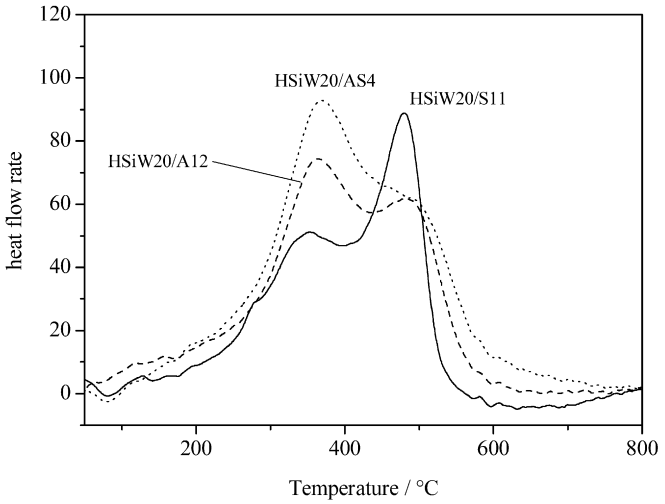

Fig. 14. DTA for spent catalysts HSiW20/A12, HSiW20/S11, HSiW20/AS4 (heating rate 10 K/min, airflow 1 l/h, 5–20 mg of catalyst).

3.10. Characterisation of spent catalysts

So far it was not possible to clarify the nature of the deposits directly on the surface of the catalysts, e.g. by means of spectroscopic methods. Nevertheless, carbonaceous deposits were formed over the surface of the catalysts during the catalytic reaction. The results from thermal analysis TG/DTA for spent catalysts HSiW20/A12, HSiW20/S11 and HSiW20/AS4 are shown in Fig. 14. Usually a weight loss of approximately 10% was measured but not included in the C-balance. A precise quantification was not carried out due to the operational mode (e.g. non-stationary regime, changes in reaction temperature, and varying measurement time). The DTA curves of the spent catalysts show two exothermic peaks near 350 and 450 °C that can be assigned to two different types of deposits. For HSiW20/S11, the peak at 450 °C is larger, indicating that more thermal stable deposits are formed. On the other side, for HSiW20/AS4 and HSiW20/A12 the less thermal stable deposit species represented by the peak at 350 °C are predominant. Hence, it should be possible to regenerate those catalysts more easily than silica-supported materials. Besides that, there are also hints in literature that porosity plays a role in deactivation, especially on sil-

ica that usually contains measurable amounts of micropores [20]. Furthermore, acidic properties seem to have a significant effect, and silica-supported heteropolyacids showed increased number of acidic sites.

During the long-term test with HSiW20/AS4 also changes in the textural properties of the surface occur. The specific surface area drops from 308 to 166 m^2/g (46% loss) and the pore volume decreases from 0.43 to 0.28 cm^3 (35% loss). This observation also proves the blocking of the surface by deposits.

4. Summary and conclusions

DTA measurements proved that the bulk HPAs are stable up to approximately 400 °C. Therefore, all supported catalysts were calcined at this temperature. When supporting the heteropolyacids over alumina, silica, and aluminosilicate, the thermal stability is even increased. The decomposition of bulk heteropolyacids showed exothermic peaks mainly due to loss of water. Alumina-supported heteropolyacids showed additional endothermic peaks indicating strong interaction between active compound and support that overweighs the previous effect. On the other side, silica-supported heteropolyacids still showed exothermic peaks due to weak interaction.

XRD results showed that reflections are only obtained on silica-supported materials where the interaction is low and permits the agglomeration of larger crystallites. Molybdenum containing solids seemed to be less thermal stable than tungsten containing compounds as XRD showed partial decomposition forming molybdenum oxide. Raman spectra also inferred the partial decomposition of molybdenum containing heteropolyacids on alumina as well as over silica. Polymolybdates and molybdenum oxide were identified as decomposition products. On the other hand, for tungsten containing supported catalysts no new Raman bands appeared, which indicates higher stability than for molybdenum containing compounds.

BET data revealed that impregnation of heteropolyacids on the surface leads to a drop in specific surface area due to plugging of the pores. Specific surface area of the silica-supported catalysts is higher, and these silica materials have a significant amount of micropores. Alumina- and aluminosilicate-supported heteropolyacids are rather mesoporous. In general, alumina support was more acidic than silica support. After impregnating these supports with heteropolyacids the acidity of the resulting catalysts reached similar values.

Four crucial parameters are responsible for the performance of heteropolyacids in the dehydration of glycerol in gas phase: the specific surface area, pore size of the support, surface acidity, and nature of the heteropolyacid.

At this stage it can be concluded first that impregnation onto supports generally strengthens the thermal stability of the heteropolyacids (depending on the availability of surface hydroxyl groups and zeta potential of the support). Immobilisation makes them effective catalysts for dehydration up to 300 °C. Expanding the specific surface area leads to a significant increase of active sites and therefore of catalyst activity. A strong dispersion effect on alumina containing materials was observed and these catalysts seem to deactivate more slowly compared to silica-supported ones. The reaction also runs on the bulk heteropolyacids and the bulk carriers, but desired product selectivity and stability are rather poor. Only supported catalysts lead to promising results. However, catalysts with a mass fraction of 20% by weight showed no advantage over samples with 10% loading. The pore size also has a strong impact on activity and selectivity. To a certain extent, the enlargement of the pores leads to an increase in performance. Shape selectivity is not expected to influence the conversion of glycerol. The surface acidity is mainly connected to the number and strength of Brønsted sites, i.e. hydroxyl groups that also seem to play a role for dispersion of the heteropolyacids on the surface of the support during preparation. However, higher acidity seems to accelerate deactivation of the catalyst. Alumina- and aluminosilicate-supported heteropolyacids were more active than silica-supported catalysts and bulk heteropolyacids. This could be due to the strong interaction between the heteropolyacids and the support surface. A strong interaction possibly leads to high dispersion of the HPAs on the surface rather than agglomeration and formation of HPA crystallites.

With all tested catalysts, acrolein was always the predominant product. Generally, all tungsten containing catalysts showed outstanding performance with regard to activity and selectivity compared to Mo and P containing materials. This can be explained by the additional redox capability introduced to the catalysts by molybdenum. The maximum selectivity for acrolein reached 75% at complete conversion on HSiW/AS4 at 275 °C. The reforming of glycerol as a possible side reaction at such conditions was completely suppressed.

With regard to application, it has to be pointed out strongly that the maximum selectivity for acrolein is obtained at complete conversion and hence a favourable single pass conversion is possible. Long-term tests up to 300 h on-stream were carried out. It is also beneficial that the catalysts could be regenerated easily in situ with a small amount of oxygen in the feed at moderately elevated temperature within a short time period.

Acknowledgments

The authors wish to thank Dr. U. Bentrup for Raman studies, Dr. M. Schneider for XRD investigations, Mrs. S. Evert for ammonia TPD analysis and Mr. R. Eckelt for TG/DTA data and nitrogen adsorption measurements. Financial support by the Egyptian Ministry of Higher Education is gratefully acknowledged.

References

[1] http://www.theglycerolchallenge.org/.
[2] A. Corma, S. Iborra, A. Velty, Chem. Rev. 107 (2007) 2411.
[3] M. McCoy, Chem. Eng. News 84 (2006) 7.
[4] P. McMorn, G. Roberts, G.J. Hutchings, Catal. Lett. 63 (1999) 193.
[5] S. Carrettin, P. McMorn, P. Johnston, K. Griffin, C.J. Kiely, G.J. Hutchings, Phys. Chem. Chem. Phys. 5 (2003) 1329.
[6] W.C. Ketchie, M. Murayama, R.J. Davis, Top. Catal. 44 (2007) 307.
[7] A. Abbadi, H. van Bekkum, Appl. Catal. A 148 (1996) 113.
[8] J. Deutsch, A. Martin, H. Lieske, J. Catal. 245 (2007) 428.
[9] T. Miyazawa, S. Koso, K. Kunimori, K. Tomishige, Appl. Catal. A 318 (2007) 244.
[10] J. Barrault, J.-M. Clacens, Y. Pouilloux, Top. Catal. 27 (2004) 137.
[11] M. Richter, Y.K. Krisnandi, R. Eckelt, A. Martin, Catal. Commun. 9 (2008) 2112.
[12] H. Adkins, W.H. Hartung, Org. Synth. Coll. 1 (1941) 15.
[13] A. Neher, T. Haas, D. Arntz, H. Klenk, W. Girke, U.S. Pat. 5 387 720 (1995).
[14] E. Schwenk, M. Gehrke, F. Aichner, U.S. Pat. 1 916 743 (1933).
[15] S. Ramayya, A. Brittain, C. DeAlmeida, W. Mok, M.J. Antal, Fuel 66 (1987) 1364.
[16] L. Ott, M. Bicker, H. Vogel, Green Chem. 8 (2006) 214.
[17] M. Watanabe, T. Iida, Y. Aizawa, T.M. Alda, H. Inomata, Bioresour. Technol. 98 (2006) 1285.
[18] S. Chai, H. Wang, Y. Liang, B. Xu, Green Chem. 9 (2007) 1130.
[19] S. Chai, H. Wang, Y. Liang, B. Xu, J. Catal. 250 (2007) 342.
[20] E. Tsukuda, S. Sato, R. Takahashi, T. Sodesawa, Catal. Commun. 8 (2007) 1349.
[21] I.V. Kozhenikov, Chem. Rev. 98 (1998) 171.
[22] J.-M. Tatibouët, C. Montalescot, K. Brückman, J. Haber, M. Che, J. Catal. 169 (1997) 22.
[23] B.K. Hodnett, J. B Moffat, J. Catal. 88 (1984) 253.
[24] R.I. Maksimovskaya, V.M. Bondareva, Zh. Neorg. Khim. [Russ. J. Chem., Engl. Transl.] 39 (1994) 1298.
[25] C. Rocchiccioli-Deltcheff, A. Aouissi, M.M. Bettahar, S. Launay, M. Fournier, J. Catal. 164 (1996) 16.
[26] R.I. Maksimovskaya, G.M. Maksimov, G.S. Litvak, Russ. J. Chem. Bull. Int. Ed. 25 (2003) 103.
[27] L.R. Pizzio, M.N. Blanco, Microporous Mesoporous Mater. 103 (2007) 40.
[28] A.A. Babad-Zakhryapin, V.P. Moiseev, Izv. Akad. Nauk SSSR, Ser. Khim. 5 (1964) 799.

[29] A.A. Babad-Zakhryapin, Izv. AN SSSR, Otd. Khim. N. (1963) 215.
[30] A.A. Babad-Zakhryapin, N.S. Gorunov, Izv. AN SSSR, Otd. Khim. N. (1963) 14.
[31] J.B. Mofatt, S. Kasztelan, J. Catal. 109 (1988) 206.
[32] K.M. Rao, R. Gobetto, A. Iannibello, A. Zecchina, J. Catal. 119 (1989) 512.
[33] C. Hu, Y. Zhang, L. Xu, G. Peng, Appl. Catal. A: Gen. 177 (1999) 237.
[34] R. Fricke, G. Öhlmann, J. Chem. Soc. Faraday Trans. I 82 (1986) 263.
[35] C. Rocchiccioli-Deltcheff, M. Amirouche, G. Hervé, M. Fournier, M. Che, J.M. Tatibouët, J. Catal. 126 (1990) 591.
[36] Y. Wu, X. Ye, X. Yang, X. Wang, W. Chu, Y. Hu, Ind. Eng. Chem. Res. 35 (1996) 2546.
[37] A. Popa, V. Sasca, E.E. Kis, R.M. Neducin, M.T. Bokorov, J. Halasz, J. Optoelectron. Adv. Mater. 7 (2005) 3169.
[38] S. Damyanova, J.L.G. Fierro, Chem. Mater. 10 (1998) 871.
[39] M. Kosmulski, Chemical Properties of Material Surfaces, Marcel Dekker, New York, 2001.
[40] A. Brückner, G. Scholz, D. Heidemann, M. Schneider, D. Herein, U. Bentrup, M. Kant, J. Catal. 245 (2007) 369.
[41] C. Rocchiccioli-Deltcheff, M. Fournier, R. Franck, R. Thouvenot, Inorg. Chem. 22 (1983) 207.
[42] P.G. Vázquez, M.N. Blanco, C.V. Cáceres, Catal. Lett. (1999) 205.
[43] M. Pope, Heteropoly and Isopoly Oxometallates, Springer, Berlin, 1983.
[44] E. Caliman, J.A. Dias, S.C.L. Dias, A.G.S. Prado, Catal. Today 107 (2005) 816.
[45] J.C. Yori, J.M. Grau, V.M. Benítez, J. Sepúlveda, J. Appl. Catal. A: Gen. 286 (2005) 71.
[46] M.J. Verhoef, P.J. Kooyman, J.A. Peters, H. Bekkum, Microporous Mesoporous Mater. 27 (1999) 365.
[47] D. Varisli, T. Dogu, G. Dogu, Chem. Eng. Sci. 62 (2007) 5349.
[48] A.G. Alejandre, P. Castillo, J. Ramírez, G. Ramis, G. Busca, J. Appl. Catal. A: Gen. 216 (2001) 181.
[49] A. Martin, F. Luck, U. Armbruster, L. Patria, J. Radnik, M. Schneider, Top. Catal. 33 (2005) 155.